# System-Integrated Finite Element Analysis of a Full-Scale Helicopter Crash Test with Deployable Energy Absorbers

Martin S. Annett

martin.s.annett@nasa.gov

Structural Dynamics Branch

NASA Langley Research Center

Hampton, VA 23681

Michael A. Polanco

michael.a.polanco@nasa.gov

ATK Space Systems

Hampton, VA 23681

## ABSTRACT

A full-scale crash test of an MD-500 helicopter was conducted in December 2009 at NASA Langley's Landing and Impact Research facility (LandIR). The MD-500 helicopter was fitted with a composite honeycomb Deployable Energy Absorber (DEA) and tested under vertical and horizontal impact velocities of 26-ft/sec and 40-ft/sec, respectively. The objectives of the test were to evaluate the performance of the DEA concept under realistic crash conditions and to generate test data for validation of a system integrated finite element model. In preparation for the full-scale crash test, a series of sub-scale and MD-500 mass simulator tests was conducted to evaluate the impact performances of various components, including a new crush tube and the DEA blocks. Parameters defined within the system integrated finite element model were determined from these tests. The objective of this paper is to summarize the finite element models developed and analyses performed, beginning with pre-test predictions and continuing through post-test validation.

## Introduction

The NASA Subsonic Rotary Wing (SRW) project is sponsoring fundamental research associated with improvements in rotorcraft crashworthiness [1]. The tasks identified under the SRW project include evaluation of a composite honeycomb Deployable Energy Absorber (DEA) [2-4], material parameter uncertainty quantification, occupant modeling, and injury risk assessment. A task was also established to develop and validate a system integrated rotorcraft finite element model (FEM), which incorporates aspects of the aforementioned tasks.

The analytical techniques necessary to reliably assess impact loads are less mature compared with other dynamic analyses required to assess other phases of rotorcraft flight. The energy absorption mechanisms of the airframe are characterized by highly nonlinear deformation, contact loading, and material response. The inclusion of all components in a single comprehensive computational model allows for

Presented at the American Helicopter Society 66th Annual Forum, Phoenix, AZ, May 11-13, 2010. 

*The use of trademarks or names of manufacturers in this report is for accurate reporting and does not constitute an official endorsement, either expressed or implied, of such products or manufacturers by the National Aeronautics and Space Administration

interactions that might be neglected when analyzing systems using separate models.

Modeling detailed representations of the frame, seats, restraints, and occupants into a single FEM is now common practice within the automotive crashworthiness community [5,6]. Prior to the mid 1990's, most impact analyses were sequentially coupled, with vehicle model responses defined as pulse inputs for occupant, seat, and restraint models. Interaction between the vehicle and occupant models required simplifying assumptions. Efforts to conduct integrated simulations have progressed along with advances in computing power.

The development of the system integrated FEM was predicated on a series of tests, ranging from the component levels to the culminating full-scale crash test. These component tests included crush tube dynamic loading, seat mesh impact testing, and MD-500 mass simulator swing tests. Finite element analyses of these tests were also performed in parallel. This hierarchical approach expanded confidence and mitigated uncertainties in component representation within the FEM.

**Full-Scale Test Article Description**

The full-scale crash test of the MD-500 helicopter was conducted at the NASA Langley Research Center (LaRC) Landing and Impact Research facility (LandIR). The LandIR facility is a 240 ft tall gantry structure with swing cables attached at one end and a movable pullback platform positioned on the opposite end. Two pullback cables raise the test article to a prescribed height. Upon pyrotechnic release of the pullback cable, the test article swings along two pairs of swing cables attached to the test article. The two pairs of swing cables are equally spaced to form a parallelogram. This configuration controls pitch, roll and yaw rate during the swing. The swing cables are pyrotechnically severed just prior to impact.

The test article used for the full-scale crash test includes an MD-500 helicopter fuselage and skid gear. The airframe was provided by the US Army's Mission Enhanced Little Bird (MELB) program. Variants of this helicopter, including the OH-6 and the MD-530, have been flown in civilian and military applications for more than 40 years.

A photograph of the test article is shown in Figure 1. The weight of the test article is equivalent to the MD-500 maximum gross weight of 3,000 lb. The empty weight is approximately 500 lb. The occupant and seat weights total 800 lb. The remainder is ballast weight representing the tail section, fuel, rotor, transmission, and engine. The weight and balance information was provided by MELB.

**Figure 1. MD-500 Test Article**

Two crew and two passenger Anthropomorphic Test Devices (ATD) are positioned in standard non-energy absorbing military seats. The crew ATDs are restrained with four point harnesses and the passenger ATDs are restrained with three-point harnesses. The pilot is a 50th percentile HYBRID III male. The co-pilot and one passenger are 50th percentile HYBRID II males. The HYBRID III ATD is modified to include a straight lumbar spine, and is similar to the lumbar spine of a HYBRID II ATD. The straight lumbar spine is used for aviation seat certification and enforces proper spinal loading for vertical impact. The second passenger is a biofidelic torso attached to a HYBRID III pelvis and legs. The biofidelic torso is the 50th percentile Human Surrogate Torso Model (HSTM50). The HSTM50 has been developed by The Johns University Applied Physics Laboratory and contains detailed representations of organs, skeletal structure and soft tissue [7].

The DEA is fabricated of Kevlar-129 fabric/epoxy and consists of multiple hexagonal cells. A typical DEA design is illustrated in Figure 2. The cell wall flat facet width is one inch. Cell wall heights vary from 16 to 20 inches. Two DEA's blocks, spanning the fuselage belly surface, were secured to the fuselage outer skin with parachute cord. The cord was restrained to the fuselage using two aluminum rails mounted below the door openings.

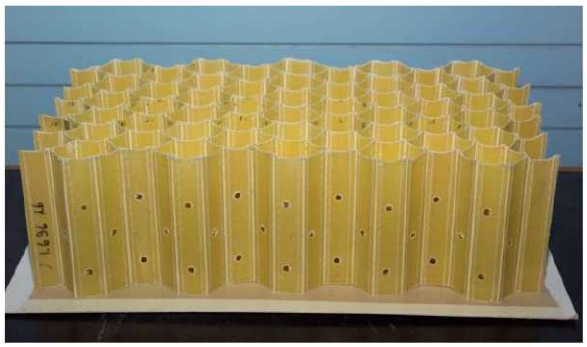

**Figure 2. DEA Design**

The MD-500 standard oleo-pneumatic struts, mounted between the skid gear and the airframe, are rated for 6 feet per second vertical impact conditions. The airframe hard points were likely to be overloaded as the struts bottom out and become rigid under the high impact velocities expected in the full-scale crash test. Consequently, the oleo struts were replaced with a set of crush tubes to absorb energy through inversion drawing. The crush tubes allow the skid gear to properly swing out on impact without being overloaded. The tubes are overwrapped with graphite epoxy, which strengthens the column buckling strength beyond the crush load. Rod ends are attached at either end of the tube to impose purely axial loads through the strut length. A summary of the crush tube design is provided in [8]. A crush tube is shown in Figure 3.

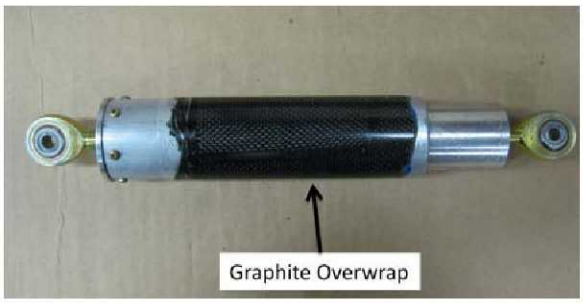


**Figure 3. Crush Tubes**

The fuselage and skid gear are instrumented with a combination of strain gages and accelerometers. ATD instrumentation includes head, chest, and pelvic accelerometers, lumbar load cells, restraint load cells, and pressure gages. A total of 160 channels of data were collected at a sample rate of 10,000 Hz. Measurements of vehicle kinematics were taken using two and three dimensional photogrammetry [9].

**Component Development**

Simulations were conducted using the nonlinear finite element analysis solver LS-DYNA [10]. LS-DYNA applies explicit time integration techniques to solve transient dynamic problems and provides the capability to handle both material and geometric nonlinearities. There are two fundamental approaches to modeling the DEA. In the first approach, the cell geometry is represented as a continuum with solid elements [11]. The material properties are elastic-plastic and orthotropic. Material orientation is along the longitudinal axis of the cell wall. At high volumetric strains, compaction occurs and the slope of the yield stress versus volumetric strain curve in the cell longitudinal direction sharply increases. For the second approach, the cell walls are represented with shell elements that are assigned elastic-plastic and isotropic material properties. The compaction of the DEA is directly replicated as the cell walls plastically hinge and fold [12]. The modeling approaches were evaluated against dynamic crush tests of DEA sections.

The solid based DEA option is attractive since the nonlinearities and crushing response are captured inherently within the material model. The shell based option requires a significantly larger number of elements, compared with the solid based option, to replicate the folding patterns accurately. The nonlinearities in the shell based option are characterized by both geometric and constitutive modeling. The energy attenuation behavior of the solid and shell based DEA models are comparable for vertical only impact conditions. However, when horizontal velocity exists at impact, the behavior of the solid based model in the in-plane shear direction is not captured adequately. The crush and deformation patterns differ between the shell and solid based models. The in-plane response of the shell based model is primarily governed by geometry. Therefore, the collapse of the cell structures and the weak in-plane shear response are intrinsic.

For the shell-based models, convergence studies revealed that the maximum acceptable element length was approximately⅓ inch. That corresponds to hundreds of thousands of elements per DEA component. Since adequate computing capacity was available and the solution time was not prohibitive, the shell based model was selected for the system integrated model. The typical mesh refinement of a shell based DEA model is illustrated in Figure 4. The material model is elastic and piecewise linear plastic with a Young's Modulus of 340 ksi and initial yield

stress of 7,500 psi. The yield stress versus plastic strain curve is plotted in Figure 5.

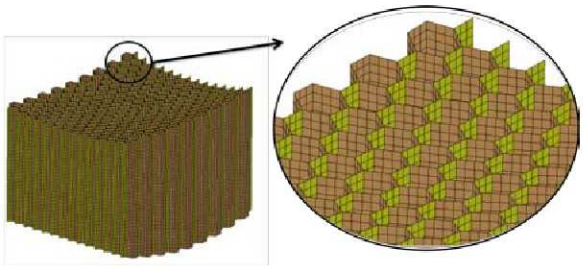

**Figure 4. Shell Based DEA FEA**

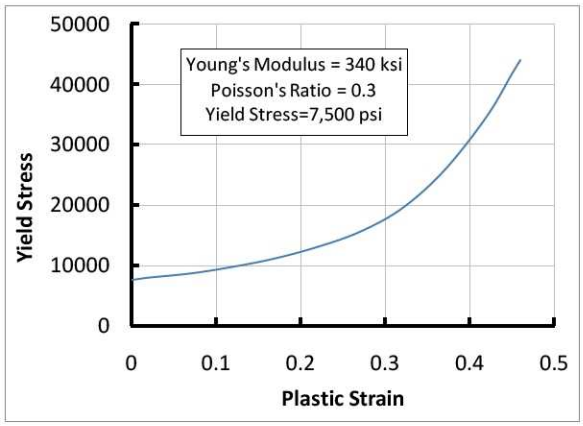


**Figure 5. DEA Material Properties**

The crush tubes are represented by truss elements that only transmit axial loads. The material property is assumed to be elastic-plastic aluminum. The crush strength versus stroke curve was determined from dynamic impact tests. The dynamic test setup and characteristic load time history are shown in Figure 6 [8]. A yield stress was defined equivalent to the dynamic crush load of 2,300 lb. A nearly perfectly plastic behavior is assumed upon attaining the crush load.

The skid gear was acquired from an MD-500 parts manufacturer. The skid gear is composed primarily of Aluminum 7075-T73 die forgings. Each skid gear is attached to a lateral support and hinged along the body centerline. The skid gear FEM was constructed based on measurements of the overall dimensions and wall thicknesses. The skid gear FEM is modeled with elastic-plastic shell elements. The total weight of the skid gear is 80 lb. The finite element model of the skid gear and struts is shown in Figure 7.

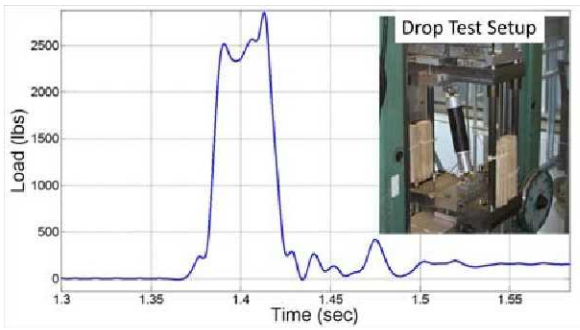


**Figure 6. Crush Tube Dynamic Testing**

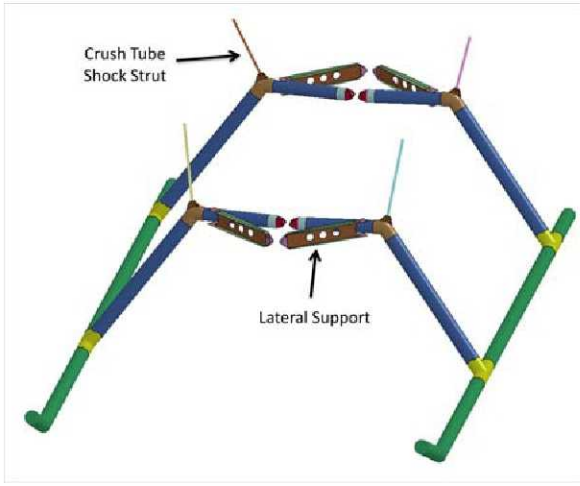


**Figure 7. Skid Gear FEM**

The performances of the skid gear, crush tubes and the DEA were verified by conducting two crash tests of an MD-500 mass simulator. The simulator is a 2,500-lb. thick aluminum plate attached to the skid gear with stainless steel brackets and lateral supports. The first mass simulator test was conducted prior to DEA fabrication. Therefore, a block of polystyrene was attached beneath the plate in place of the DEAs. The mass simulator was instrumented with a triaxial accelerometer at the center of gravity (CG) and uniaxial strain gages on the vertical tubes of the skid gear. For the first swing test, the vertical and horizontal impact velocities were 18-ft/sec and 28-ft/sec, respectively. These velocities roughly represent half the kinetic energy of the full-scale crash conditions. The test was configured for zero pitch, roll, and, yaw angles. The actual angles at impact were slightly off attitude. The pitch, yaw, and roll attitudes were 1.8, 6.7, and 3.4 degrees, respectively. The MD-500 mass simulator test article and FEM are shown in Figure 8.

The polystyrene FEM was modeled with a crushable foam material model and was tied directly to the aluminum plate. The concrete surface was represented with a planar rigid wall. The brackets and lateral supports were hinged and pinned with rigid revolute joints to represent the kinematic interface between the skid gear and the helicopter.

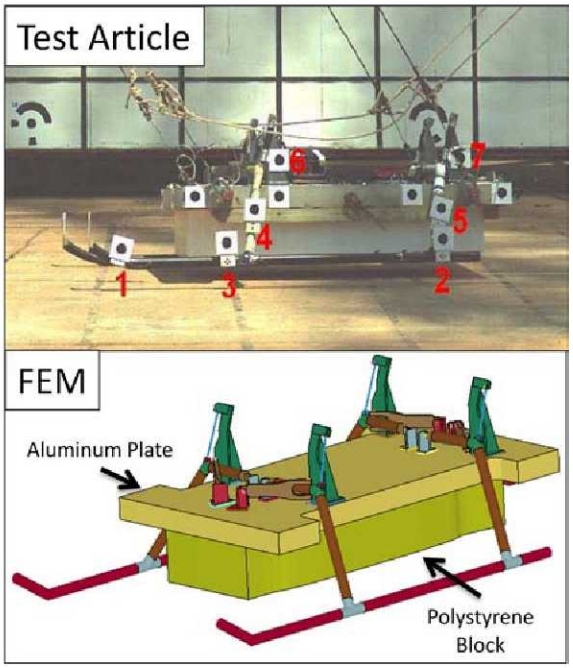


**Figure 8. MD-500 Mass Simulator with Foam**

LS-DYNA acceleration results of the mass simulator/foam test are plotted against the test data in Figure 9. The acceleration results were filtered with a Butterworth (BW) 50 Hz low pass filter. The net CG accelerations indicate slight discrepancies during the skid gear impact phase of the impact occurring between 0.01 and 0.02 seconds. The LS-DYNA model presumes a nearly perfectly plastic tangent modulus for the vertical struts, whereas the test data indicates a stiffness increase that is reflected in the higher acceleration peaks. The foam energy absorption phase of the impact, which is represented in the vertical acceleration component, shows good agreement. The horizontal acceleration component relates to the slide out response. The analysis shows higher horizontal loads as the foam impacts the surface. The friction coefficient was subsequently lowered to reflect the test data.

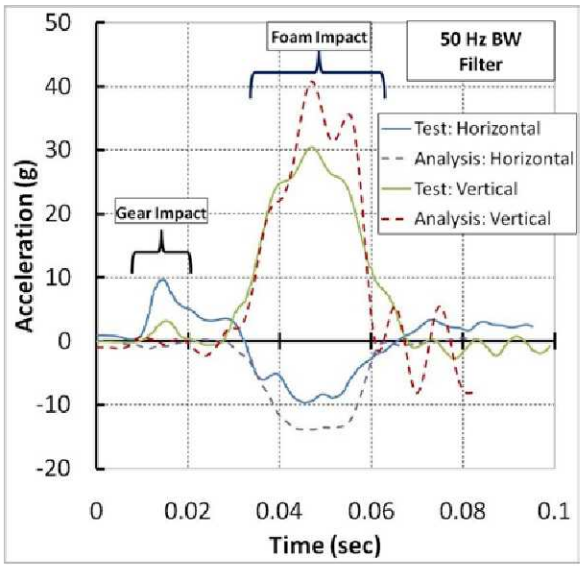


**Figure 9. Comparison of Test and Analysis Accelerations for the Mass Simulator with Foam**

The maximum and minimum axial strains for the right forward vertical leg of the skid gear are shown in Figure 10. The vertical members are highly loaded upon impact and exhibit a tension/compression response due to bending. The surface of the tube furthest from the centerline is the outboard face which is under compression. The opposite surface of the tube is the inboard face and is in tension. The strains do not exceed the yield allowable of the aluminum and no plastic deformation was observed from the post-test examination of the skid gear. The analysis and test strains are in reasonable agreement. The modeling approach for the skid gear and the crush tubes was deemed adequate based on these results.

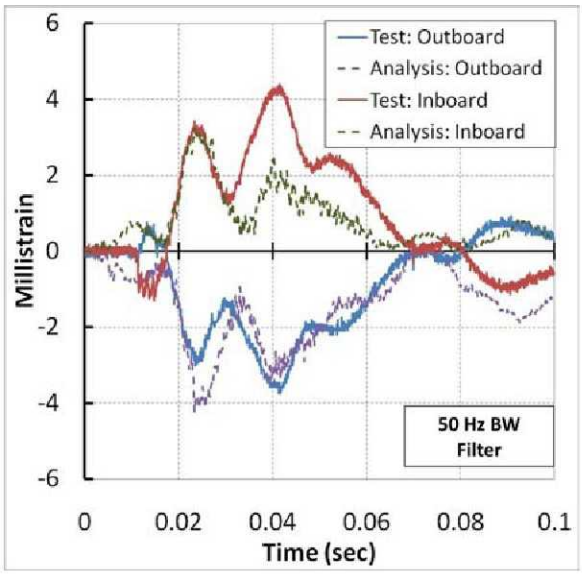


**Figure 10. Comparison of Test and Analysis Strains for the Mass Simulator with Foam**

The second mass simulator swing test was conducted at the full-scale vertical and horizontal impact velocities of 26-ft/sec and 40-ft/sec, respectively. The foam was replaced by two DEA segments. The height of the DEA is approximately 14 inches with the bottom surface of the DEA positioned just above the skid gear. Each segment was secured to the underside of the flat plate with parachute cord. Based on results from parametric studies of the DEA [11,12], the orientation of the DEA segments was set at 20 degrees from vertical. The test article and corresponding FEM are shown in Figure 11. The pitch, roll, and yaw angles were negligible compared to the first mass simulator test. Pitch was zero, roll angle was 1.5 degrees, and yaw angle was 1.6 degrees.

For the mass simulator/DEA FEM, the skid gear to plate interfaces remained unchanged from the mass simulator/foam FEM. The DEA's were fixed to the underside of the plate surface using a tied contact algorithm. A single surface contact was defined for the DEA to provide interaction between folded and crushed shell elements.

The vertical and horizontal acceleration data are plotted against the analysis results in Figure 12. As with the first mass simulator test, the acceleration results were filtered with a Butterworth 50 Hz low pass filter. The results indicate similar pulse durations of 0.08 seconds. The test results show two distinct peaks within that window. The initial crush load is approximately 12.5 g and the compaction load reaches 18 g. The analysis results show a uniform crush load of approximately 15 g. The total permanent DEA compaction measured from the test was 11 inches, while the analysis model vertical compaction ranged between 7 and 8 inches.

The horizontal motion is primarily a function of the DEA slide out along the concrete. Results from slow-rate friction drag tests performed on representative DEA sections indicated a friction coefficient of 0.5. Based on the measured horizontal accelerations, the friction coefficient of 0.5 specified in the rigid wall definition was too conservative. The friction coefficient was reduced to 0.3 for all subsequent simulations with the DEA.

The axial strains for the right forward vertical leg of the skid gear are shown in Figure 13. Similar to the first mass simulator test, the vertical tubes initially compress and then bend outward as the gear slides along the concrete. Most of the loads are carried through the DEA; therefore the strains in the gear are low and elastic. Strain results compare well between test and analysis.

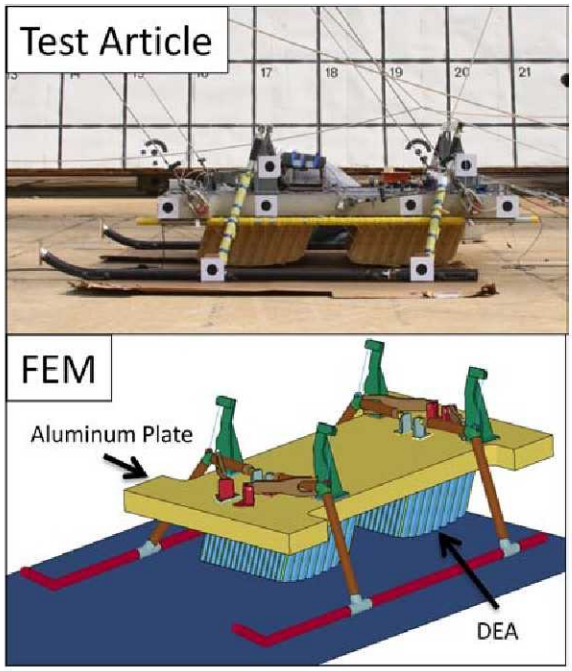


**Figure 11. MD 500 Mass Simulator with DEA**

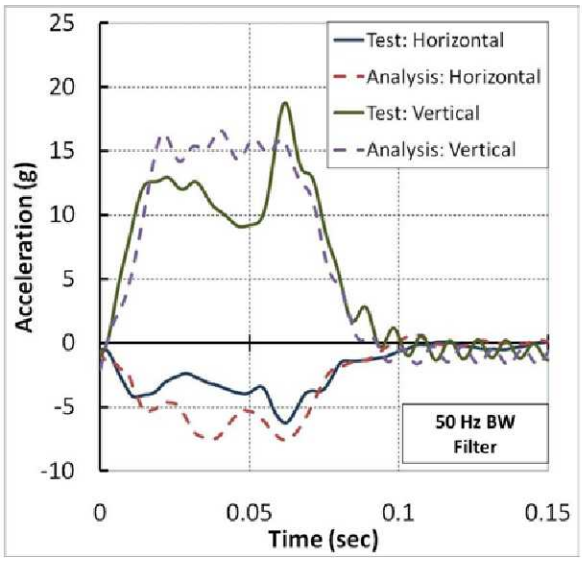


**Figure 12. Comparison of Test and Analysis Accelerations for the Mass Simulator with DEA**

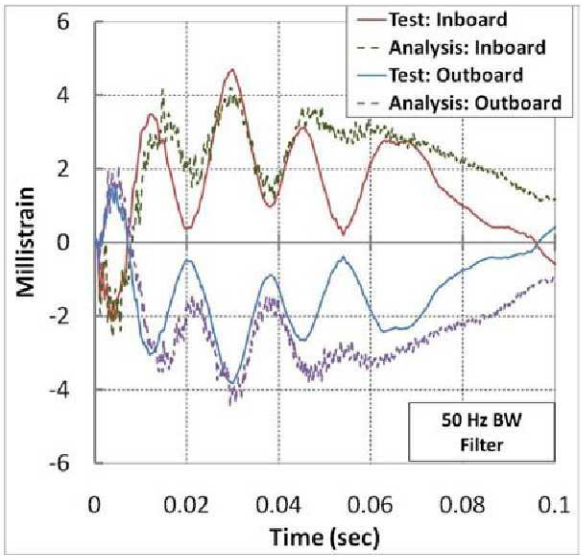


**Figure 13. Comparison of Test and Analysis Strains for the Mass Simulator with DEA**

Results from the two mass simulator tests validated the DEA, skid gear, and crush tube models. In preparation for the full-scale crash test, the MD-500 FEM was constructed. Attention was given to the components susceptible to damage during impact, namely the fuselage and seats.

**MD-500 Fuselage Model Description**

A computer aided design (CAD) model of the MD-500 fuselage was provided by the Army Aviation Applied Technology Directorate (AATD). The geometry model consisted of surface representations of the fuselage outer mold line (OML), bulkheads, seat pan, and floor. A more comprehensive geometry was desired that captured the internal primary and secondary structures and could be seamlessly meshed into an FEM. Geometry that contains compatible surface edges eliminates the need to manually manipulate and merge nodes. The model must contain enough detail to represent the expected plastic deformation and accurately transmit loads into the seats and occupants. This underlying geometry provides the foundation for more refined meshing or parameter studies.

Ribs and stiffeners not present in the baseline geometry model, were measured and added to the existing geometry. Thickness measurements were taken using ultrasonic transducers and calipers. The skin thicknesses typically ranged from 0.02 to 0.04 in. The keel beam, a critical shear load path for the subfloor, was added. Material densities were scaled to represent the mass of additional ribs and stiffeners not discretely modeled.

The LS-DYNA FEM of the MD-500 fuselage is shown in Figure 14. The DEA and skid gear models consist of approximately 320,000 elements. The element count for the fuselage was targeted to not exceed 500,000 elements, including seats and occupants. The size of the fuselage model is 27,000 elements. Refinement is concentrated around the subfloor. The fuselage model is primarily composed of shell elements representing airframe skins, ribs and stiffeners. Ballast representing rotor mass, tail mass, and fuel is incorporated in the FEM as concentrated mass elements. The lifting and pullback fixtures were added as rigid shells. The platform that supports the data acquisition system (DAS) was mounted in the tail and also modeled as a rigid shell. The original geometry contained a blunt nose. The FEM was modified to a chine nose to represent the actual fuselage.

Material properties for the fuselage are based on the MD-500 Structural Repair Manual [13]. The fuselage material is primarily Aluminum 2024-T3, and has elastic-plastic properties. The nose is composed of fiberglass, and the engine fairing is composed of Kevlar fabric.

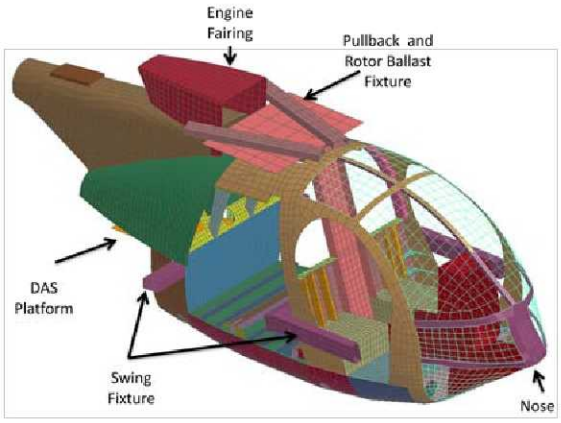


**Figure 14. MD-500 Fuselage FEM**

## Crew Seat Model Description

Two crew seats and a single passenger bench seat were provided by an MD-500 parts supplier. The seats are standard military issue with aluminum frames and nylon mesh fabric stretched over the frames. The seat geometries were constructed using target tracking 3-D photogrammetric techniques. Targets were attached to the seat and point clouds were generated from images of the targets. The point clouds were converted to parametric solids, which were used to generate a finite element mesh. The modeling process for the crew seat is illustrated in Figure 15, with both crew seat and passenger bench FEM's included.

The seat fabric material properties were determined by dynamic drop tests of a 20-lb hemispherical mass onto the fabric. Vertical acceleration was measured by an accelerometer mounted within the drop mass. The drop test was simulated with an FEM. The modulus of the material was modified to match test accelerations. Figure 16 shows the drop test setup, FEM simulation, and acceleration data comparison. The calculated effective dynamic modulus is 4,000 psi. This modulus is almost three times higher than the modulus determined from quasi-static load cell testing.


**Figure 15. Seat FEM**

The as-received passenger bench seat is attached to the floor and rear bulkhead in four locations. This mount is vulnerable to structural failure at the rear seat pan tubes during impact. Additional bracing is used for military applications at the front edge of the seat pan, which precludes this collapse. Support braces were added to the seat from the front edge to the floor. Rigid links representing this attachment scheme were used in the FEM.

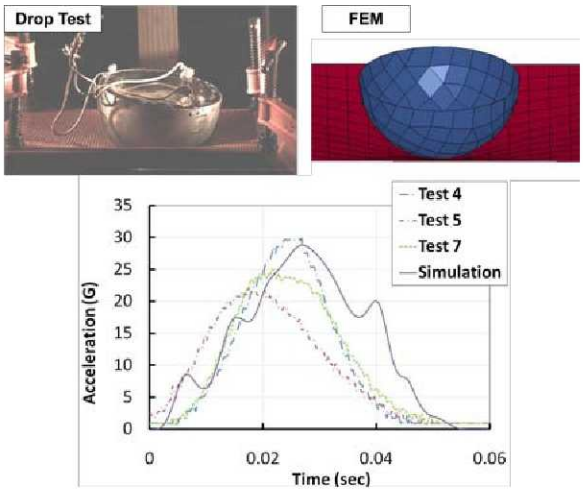


**Figure 16. Seat Fabric Dynamic Testing**

## Occupant Model Description

A model of the 50th percentile HYBRID III male was used for the HYBRID II and III ATDs [14] and is denoted the LSTC FEM. The models contain mostly

rigid representations of the ATD components. Ribcage, neck, jacket, and pelvis are deformable. Springs and dampers are defined at neck and limb joints. The FEMs are easily imported and positioned within the LS-DYNA pre-processor. The LSTC FEM is shown in Figure 17. Each ATD FEM contains 4,295 elements with a wide range of element types and joint definitions.

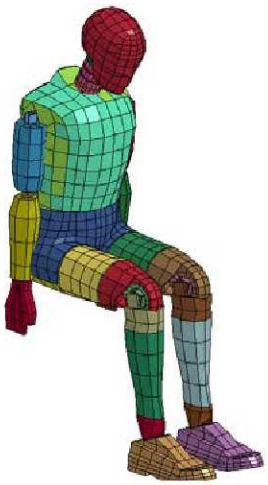

**Figure 17. LSTC HYBRID III FEM**

The biofidelic HSTM50, containing thoracic organs, skeletal structure, and soft tissue, is mated to a HYBRID III pelvis and legs and seated within the passenger compartment [7]. A reduced human torso FEM was constructed and adapted from the Human Torso Finite Element Model (HTFEM) [15]. The organs and soft tissue elements are represented by solid silicone elements. The sternum, ribcage, vertebrae and scapula are modeled with fiberglass bar and shell elements. The bar and shell elements are embedded within the solid elements and coupled with constraint algorithms. The reduced human torso FEM was attached to the LSTC FEM pelvis and legs, as shown in Figure 18.

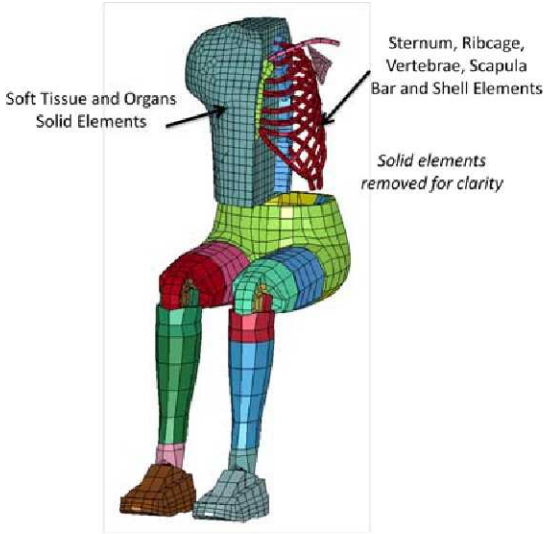


**Figure 18. Reduced Human Torso FEM**

The pilot and co-pilot ATDs are restrained with four point harnesses and the passenger and HSTM50 are restrained with three point harnesses. The seat belts were modeled with shell elements and rigid links at the retractor, attachment, and buckle interfaces. The belts were fitted to the torso and pelvis within LS-PREPOST.

The system-integrated FEM of the MD-500 is shown in Figure 19. The FEM has approximately 400,000 elements. The total weight of the test article and the FEM is 2,930 lb.

**Figure 19. MD-500 FEM**

**MD-500 Pre-Test Analysis**

Pre-test simulations were conducted with the system integrated FEM to identify potential damaged regions and to predict occupant loads. Throughout the model

development process, the mesh was locally refined and detail was added to the fuselage FEM to ensure all critical loads paths were captured. Modifications were made to the test article to limit damage and provide minimal reinforcement. Preliminary simulation results indicated extensive indentations of the belly skin as the DEA compacted. A doubler composed of four layers of 0.010 in. thick graphite epoxy fabric was bonded to the belly skin. The orientation of the rear DEA was changed from 20 degrees to zero degrees since the belly centerline was angled away from the surface. This optimized the line of action between the DEA, the surface, and the belly, and mitigated the load imparted by the rear DEA.

There was concern that the compliance of the seat fabric would cause the pelvis of the pilot and co-pilot to impact the seat box, which is the airframe structure directly underneath the seat pan. To minimize the effect of the ATD pelvis impacting the seat box, a foam wedge was placed underneath the co-pilot seat. The co-pilot seat would presumably track the seat box response more closely.

The energy absorption of the DEA is dependent upon the extent of cell wall crushing. As such, the vertical acceleration responses within the fuselage and the ATD pelvic acceleration and lumbar load response correspond directly to DEA effectiveness. The lateral and longitudinal responses are relatively benign, and will not be discussed further.

The average vertical accelerations at the semi-rigid swing fixture are shown in Figure 20 for simulations with and without the DEA. The plane of the swing fixture is near the vertical CG position of the test article [Figure 14]. With the DEA, the average load at the swing fixture is nearly 10 g with duration of roughly 90 milliseconds. The peak acceleration for the case without the DEA exceeds 30 g with duration of 60 milliseconds. The addition of the DEA reduces the peak load by about two-thirds.

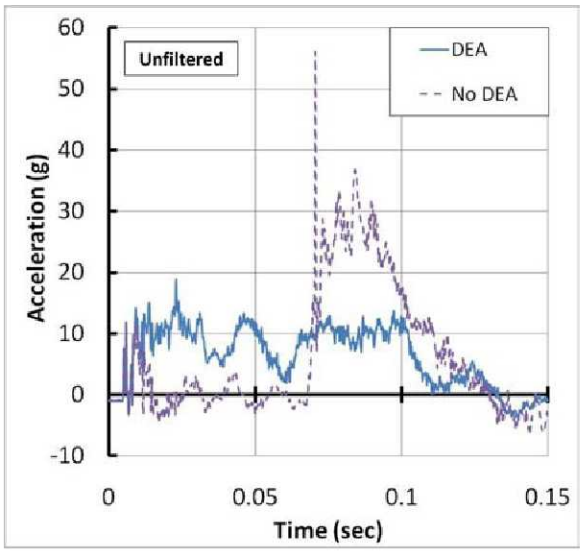


**Figure 20. Pre-Test Analysis Comparisons of Vertical Accelerations at Swing Fixture**

Severe accelerations in the direction parallel to the spine could lead to spinal compression fracture. The pre-test vertical pelvic accelerations are plotted for all four ATDs in Figure 21. The passenger and HSTM50 pelvic loads track the response of the swing fixture, with slightly higher magnitudes (15 g versus 10 g). The pilot and co-pilot loads are notably higher, with 22 to 25 g initial peaks. There is a time delay between the pilot and co-pilot response as the co-pilot seat interacts with the foam wedge earlier than the pilot impacts the seat box, but the peak acceleration is not reduced by the presence of the foam wedge.

Based on the Aircraft Crash Survival Design Guide [16], the human tolerance level for loads directed along the spinal axis is 20-25 g. The pre-test predictions show that the occupant responses with the DEA are within this limit. An additional criteria associated with spinal injury is specified in FAR Part 27.562 [19]. The compression load threshold is 1,500 lb. The lumbar loads for the pilot, co-pilot, and passenger are plotted in Figure 22. The peak lumbar loads are 800 lb, well within the 1,500 lb allowable.

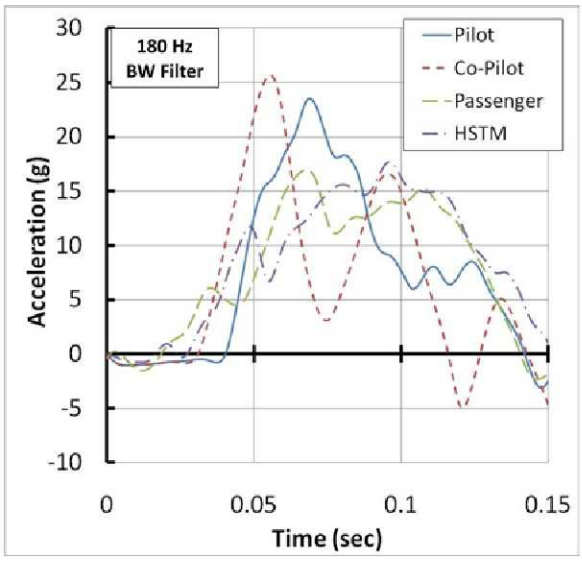


**Figure 21. Pre-Test Analysis of ATD Vertical Pelvic Accelerations**

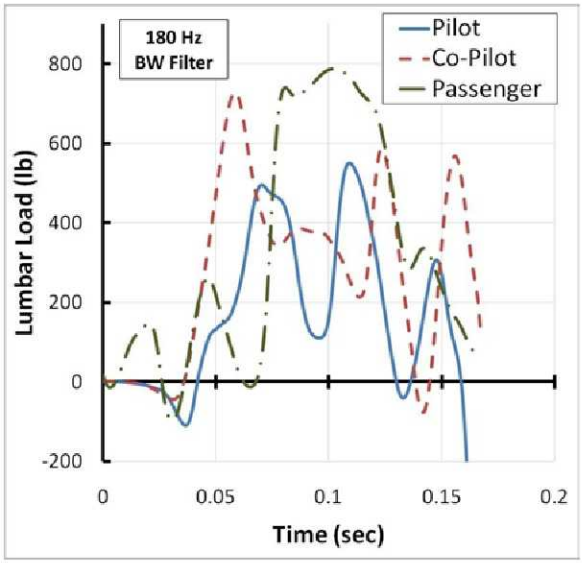


**Figure 22. Pre-Test Analysis of ATD Vertical Lumbar Loads**

## MD-500 Full Scale Test

The full-scale test was conducted in December 2009 at the LandIR facility at LaRC. The vehicle displacement time history was recorded using 2-D and 3-D photogrammetry [9]. The test article impacted with 38.7 ft/sec horizontal and 25.5 ft/sec vertical velocity, and 5.7 degrees pitch, 9.3 degrees yaw, and 7 degrees roll. The off attitude impact conditions are attributed to a combination of factors including inconsistent swing cable preloads and longitudinal offset between the swing cable effective line of action and the CG.

Overall, the damage to the test article was minor. Impact occurred initially on the front right skid gear. Slight tears in the skin above the fuselage opening were evident for both skid gears. The DEA restraint support rail impeded the gear from additional movement with the result that the right gear bent along the rail. Damage along the fuselage belly was limited to the right front section of belly forward of the front bulkhead.

The MD-500 FEM was reoriented to the test impact conditions. Additionally, the crush tubes were redefined to include rotational stiffness not present in the pre-test simulations. The overall rotation of the struts is restricted by the rod end fittings and mating clevises. This locking effect is not seen in the zero pitch, roll and yaw cases where the DEA does not fully compact. For the test orientation, the DEA along the right side nearly bottoms out and the lack of strut rotational stiffness causes the fuselage to roll to the right side. This roll motion was not observed during the impact and slide out. A six degree of freedom discrete beam was substituted with an axial load versus deflection curve equivalent to the elastic/plastic curves and bending moment versus rotation curves that include a stop angle of 10 degrees.

## Test and Analysis Comparison

A detailed summary of the test responses is provided in [8]. The test impact orientation and deformation at peak load is shown for test and analysis in Figure 23. The global deformation pattern of the DEA is similar to the deformation observed in the high speed video, primarily folding on the right side and crushing on the left side. However, upon further examination, the locations where the DEA folded and compacted and consequently transferred high impact loads locally do not correlate. The damage to the front right side did not occur in the analysis simulation. Within the simulation, dimpling of the skin occurred in the region above the rear DEA, whereas the post-test inspection revealed no damage. The DEA folding, crushing, and sliding along the belly was partially captured with the shell-based model. The addition of lateral loading within the DEA contributed to this behavior.

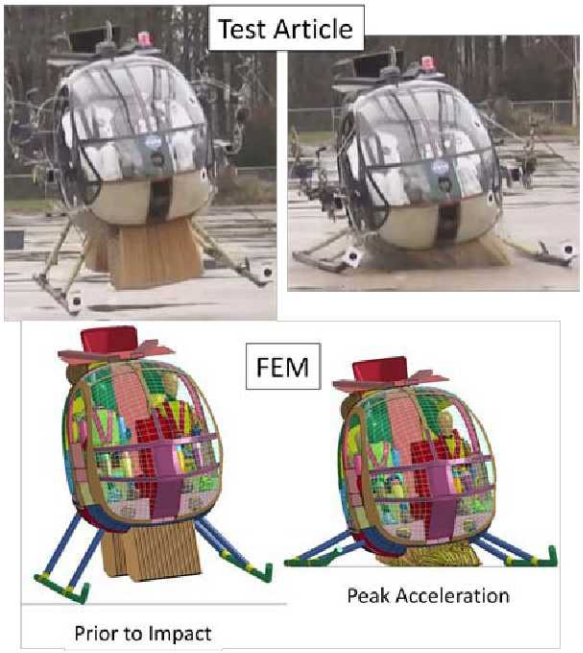


**Figure 23. Comparison of Test and Analysis MD-500 FEM Deformations**

The test acceleration pulse shapes are effectively trapezoidal with duration of roughly 0.12 seconds. All acceleration and force data are low-pass filtered with a Butterworth 180 Hz filter. No accelerometers were positioned near the vehicle CG. Therefore, an overall global acceleration was derived from photogrammetric velocity output of a target located near the CG. This acceleration was plotted with the average vertical acceleration of the swing fixture in Figure 24. There is good agreement in terms of magnitude and impulse for the fuselage.

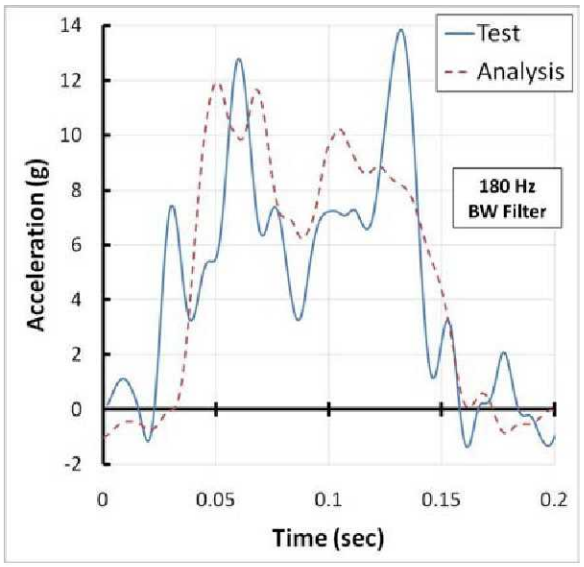


**Figure 24. Comparison of Test and Analysis Global Vertical Accelerations**

The strain response of the left front skid gear vertical tube was elastic and no damage was evident. Test and analysis results for left front vertical tube strain were comparable. The right front skid gear vertical tube strain differed between test and analysis as the tube plastically deformed. A comparison of plastic strain was not feasible since the strain gauge range was ±5 millistrains and test data was restricted to the elastic region.

The nodal vertical acceleration on the pilot seat box is plotted against test data in Figure 25. The reference coordinate system for the simulation and the test are fixed along the floor surface. The axis perpendicular to the floor represents vertical. The measured and analysis accelerations are comparable with a single sharp peak present in the analysis. Figure 26 shows the comparison of pilot ATD vertical pelvic acceleration. The measured ATD pelvic acceleration is approximately 10 g and more uniformly spread than the analysis acceleration. This load is considered survivable and within the level of voluntary exposure [16]. The higher peak load seen in the analysis possibly indicates that the pilot dummy preload is not properly pre-tensioned against the seat mesh and spurious impact loads are imparted between the ATD and seat and seat box.

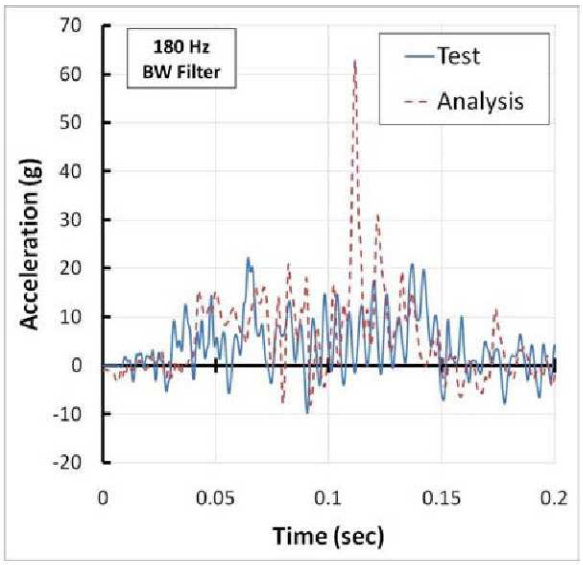


**Figure 25. Comparison of Test and Analysis Pilot Seat Box Vertical Accelerations**

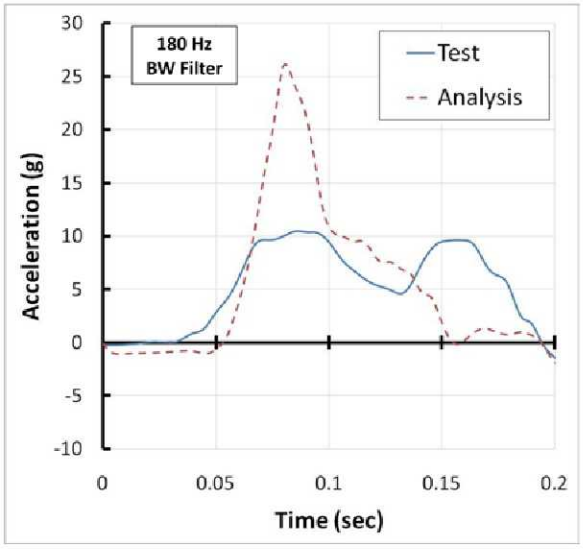


**Figure 26. Comparison of Test and Analysis Pilot Pelvic Vertical Accelerations**

The measured and analysis pilot lumbar loads are plotted in Figure 27. The test data indicated that the peak loads are well within the 1,500-lb injury criteria. The measured loads considerably exceed the analysis loads and the overall responses differ. Also evident in Figure 26 and Figure 27, the measured pulse shapes for the lumbar loads and the pelvic accelerations are similar for the pilot. The lumbar loads could consequently be computed from the pelvic accelerations. This was necessary for the HSTM50 since it did not contain a lumbar load cell. The pilot LSTC FEM does not produce similar pulse shapes between lumbar load and pelvic acceleration, and the load transfer through the pelvic region is not adequately characterized.

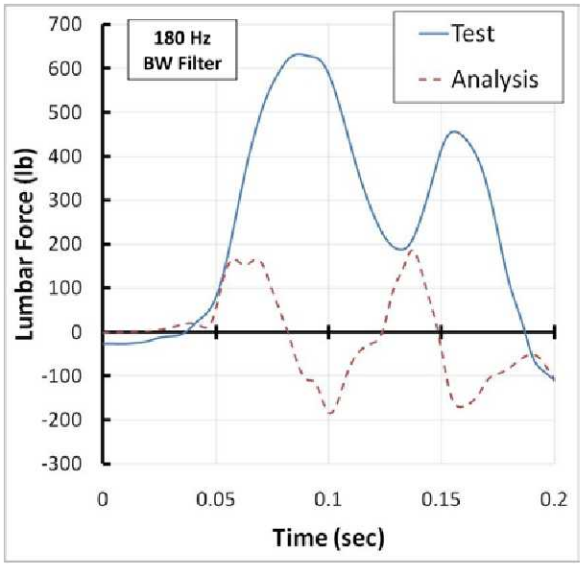


**Figure 27. Comparison of Test and Analysis Pilot Lumbar Loads**

The nodal vertical acceleration on the floor centerline beneath the passenger seats is plotted against test data in Figure 28. This location relates to the input to the passenger bench seat. The accelerations and pulse shapes compare well, with magnitudes between 12 and 17 g. The passenger pelvic accelerations and lumbar loads are shown in Figure 29 and Figure 30, respectively. The analysis responses have differing magnitudes and pulse shapes for both pelvic vertical acceleration and lumbar load as compared to test. In spite of the discrepancy between test and analysis responses, the passenger LSTC FEM does produce similar pulse shapes relating lumbar load to pelvic acceleration.

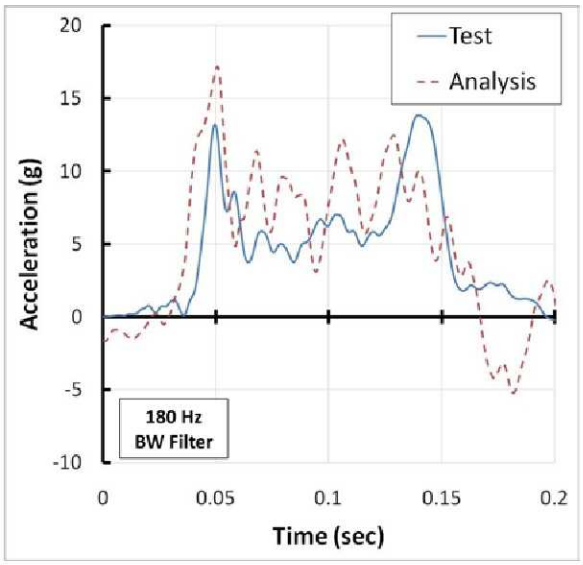


**Figure 28. Comparison of Test and Analysis Passenger Floor Vertical Accelerations**

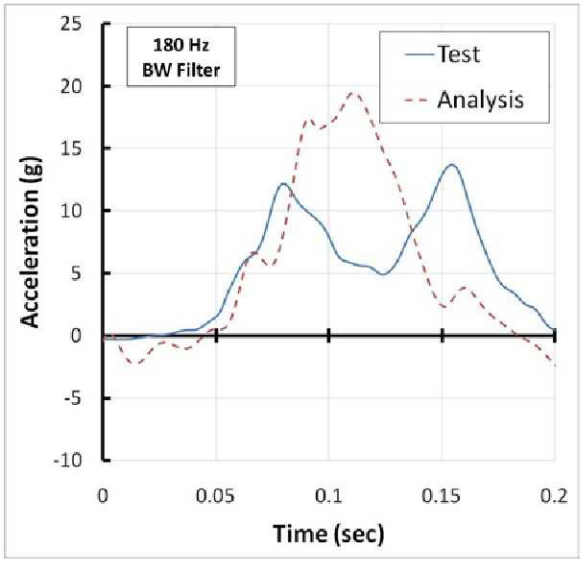


**Figure 29. Comparison of Test and Analysis Passenger Pelvic Vertical Accelerations**

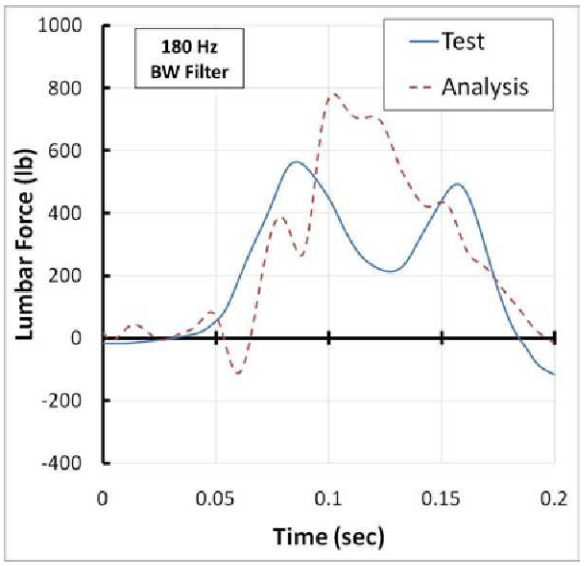


**Figure 30. Comparison of Test and Analysis Passenger Lumbar Loads**

The inconsistencies in ATD responses may be due to the ATD models alone or the complex interaction between the ATD, seat, and restraint. The LSTC FEM's have been calibrated for frontal impacts conditions. Test and analysis correlation efforts for vertically loaded seated occupants are in their initial stages. Sled tests with the seat backs oriented parallel to the track were conducted by Tabiei *et al* [19]. Several ambiguities were discovered for acceleration and force data and analysis correlation was highly sensitive to dummy and restraint positioning. Further investigation is required to resolve these discrepancies.

## Conclusion

A system integrated FEM has been developed concurrently with a full-scale crash test of an MD-500 helicopter. The fuselage model was adapted from baseline OML geometry and augmented to include skid gear and seats. The model also contains a shell based version of the DEA, three 50$^{th}$ percentile HYBRID III male ATD FEM's, and a fourth biofidelic torso/HYBRID III pelvis FEM.

Component level analyses and tests were conducted to establish the material properties of the DEA, the crush tubes, and the seat mesh. Full-scale mass simulator tests were conducted to develop confidence in both analysis and test methodologies and to reduce risk. Good agreement for skid gear strains and CG accelerations was seen between test and analysis. A pre-test simulation revealed minimal damage to the

fuselage, and occupant loads that were within the survivable injury limits.

Following the full-scale test, minor damage was observed to the skid gear and front right belly. The vehicle vertical accelerations were attenuated to peaks of 10-15 g, signifying excellent performance by the DEA's despite the off-nominal attitude at impact. The fuselage accelerations matched well between test and analysis. There were discrepancies between test and analysis for occupant loads. These ATD FEM models must be studied further for the vertical impact loading conditions considered here. The system integrated FEM has proven to be a valuable and effective predictive tool that can account for multiple crashworthy rotorcraft elements and their critical interactions.

**References**


1. Jackson, K.E., Fuchs, Y., and Kellas, S., "Overview of the NASA Subsonic Rotary Wing Aeronautics Research Program in Rotorcraft Crashworthiness," Journal of Aerospace Engineering, Special Issue on Ballistic Impact and Crashworthiness of Aerospace Structures, Volume 22, No. 3, July 2009, pp. 229-239.
2. Kellas S., "Deployable Rigid System for Crash Energy Management," US Patents 6,755,453, June 29, 2004, 6,976,729 December 20, 2005, and 7,040,658 May 9, 2006.
3. Kellas, S., and Jackson, K.E., "Deployable System for Crash-Load Attenuation," Proceedings of the 63rd AHS Annual Forum, Virginia Beach, VA, May 1-3, 2007.
4. Kellas S. and Jackson K.E., "Multi-Terrain Vertical Drop Tests of a Composite Fuselage Section," Proceedings of the 64th AHS Annual Forum, Montreal, Canada, April 29, May 1, 2008.
5. Khalil, T.B. and Sheh, M.Y., "Vehicle Crashworthiness and Occupant Protection in Frontal Impact by FE Analysis – An Integrated Approach", Proceedings of Crashworthiness of Transportation Systems: Impact and Occupant Protection, Kluwer Academic Publisher, pp. 363-399, 1997.
6. Kan, C.D., Marzougui, D., Bahouth, G. T., and Bedewi, N. E., "Crashworthiness Evaluation using Integrated Vehicle and Occupant Finite Element Models," International Journal of Crashworthiness. Vol. 6, no. 3, pp. 387-397. 2001
7. Roberts, J., Merkle, A., Biermann, P., Ward, E., Carkhuff, B., Cain, R., and O'Connor, J., "Computational and Experimental Models of the Human Torso for Non-Penetrating Ballistic Impact", Journal of Biomechanics, 40 (1), 2007, pp. 125-136.
8. Kellas, S., Jackson, K., and Littell, J., "Full Scale Crash Test of a MD 500 Helicopter with Deployable Energy Absorbers," Proceedings of the 66th AHS Annual Forum, Phoenix, AZ, May 11-13, 2009.
9. Littell, J., "Large Field Photogrammetry Techniques in Aircraft and Spacecraft Impact Testing," SEM Annual Conference & Exposition on Experimental and Applied Mechanics, Indianapolis IN, June 2010.
10. Hallquist, J., "LS-DYNA Keyword User's Manual," Version 971, Livermore Software Technology Company, Livermore, CA, August 2006.
11. Jackson, K. E., A Parametric Study on a Solid-Based Model of a Kevlar/Epoxy Composite Honeycomb," AHS Technical Specialists Meeting on Rotorcraft Structures and Survivability, Williamsburg, VA, October 27-29, 2009
12. Polanco, M., "A Parametric Study on a Shell-Based Model of a Kevlar/Epoxy Composite Honeycomb," AHS Technical Specialists Meeting on Rotorcraft Structures and Survivability, Williamsburg, VA, October 27-29, 2009
13. Anon, Structural Repair Manual, CSP–SRM–6, MD Helicopters, Inc, Mesa, AZ, May 2006.
14. Guha, S., Bhalsod, D., and Krebs, J., "LSTC Hybrid III Dummies, Positioning & Post-Processing, Dummy Version: LSTC.H3.103008_v1.0," LSTC Michigan, October 30, 2008
15. Roberts, J., Merkle, A., Biermann, P., Ward, E., Carkhuff, B., and O'Connor, J., "Modeling the Human Torso to Study BABT," Journal of Biomechanics, Volume 40, Supplement 2, August 2007, S47.
16. Desjardins, S., Laananen, D., Singley, G., "III: Aircraft Crash Survival Design Guide," USARTL-TR-79-22A, Applied Technology Laboratory, US Army Research and Technology Laboratories, Ft. Eustis, VA, 1979.
17. Code of Federal Regulations, Federal Aviation Regulations for Aviation Maintenance Technicians FAR AMT, Part 27 Airworthiness Standard: Normal Category Rotorcraft, 27.562 Emergency Landing Dynamics.
18. Kellas, S., Jackson, K., and Littell, J., "Full Scale Crash Test of a MD-500 Helicopter with Deployable Energy Absorbers," Proceedings of the 66th AHS Annual Forum, Phoenix, AZ, May 11-13, 2009.

19. Tabiei, A., Lawrence, C., and Fasanella, E., "Validation of Finite Element Crash Test Dummy Models for Predicting Orion Crew Member Injuries During a Simulated Vehicle Landing," NASA/TM—2009-215476, March 2009.